

# **Nghiên cứu phân tán vật liệu $\text{SiO}_2/\text{g-C}_3\text{N}_4$ trên nền polyvinylidene fluoride và hoạt tính quang xúc tác phân hủy dung dịch RhB trong môi trường nước**

## **TÓM TẮT**

Vật liệu  $\text{SiO}_2/\text{g-C}_3\text{N}_4$  được phân tán lên màng polyvinylidene fluoride (PVDF) bằng phương pháp đảo pha thu được màng quang xúc tác phân hủy chất màu hữu cơ rhodamine B (RhB) trong môi trường nước dưới vùng ánh sáng khả kiến. Hình thái, cấu trúc và hoạt tính quang xúc tác của các vật liệu đơn và composite phân tán lên màng PVDF được đánh giá. Với vật liệu composite  $\text{SiO}_2/\text{g-C}_3\text{N}_4$  có tính chất xốp hơn, có nhiều vị trí khuyết tật hơn so với các vật liệu  $\text{SiO}_2$  hay  $\text{g-C}_3\text{N}_4$  đơn chất khi phân tán lên màng làm cải thiện đáng kể hiệu quả quang xúc tác của vật liệu. Cụ thể, hiệu suất phân hủy RhB khỏi màng composite  $\text{SiO}_2/\text{g-C}_3\text{N}_4/\text{PVDF}$  dưới tác động của ánh sáng khả kiến đạt 81,35% vượt trội hơn so với  $\text{g-C}_3\text{N}_4/\text{PVDF}$  (46,07%) và  $\text{SiO}_2/\text{PVDF}$  (14,79%). Do đó, nghiên cứu này được kỳ vọng sẽ mở rộng triển vọng trong lĩnh vực công nghệ lọc màng.

**Từ khóa:**  $\text{SiO}_2$ ,  $\text{g-C}_3\text{N}_4$ ,  $\text{SiO}_2/\text{g-C}_3\text{N}_4$ ,  $\text{PVDF}$

# Study on dispersion of $\text{SiO}_2/\text{g-C}_3\text{N}_4$ on polyvinylidene fluoride substrate and photocatalytic activity in decomposing RhB solution in aqueous environment

## ABSTRACT

$\text{SiO}_2/\text{g-C}_3\text{N}_4$  material was dispersed onto polyvinylidene fluoride (PVDF) membrane by the phase inversion method to obtain a photocatalytic membrane for decomposing organic dye rhodamine B (RhB) in aqueous medium under visible light. The morphology, structure, and photocatalytic activity of single and composite materials deposited on PVDF membranes were evaluated. With  $\text{SiO}_2/\text{g-C}_3\text{N}_4$  composite material having more porous properties and more defect locations than single  $\text{SiO}_2$  or  $\text{g-C}_3\text{N}_4$  materials when dispersed onto the membrane, the photocatalytic efficiency of the material is significantly improved. Specifically, the degradation efficiency of RhB from  $\text{SiO}_2/\text{g-C}_3\text{N}_4/\text{PVDF}$  composite membrane under the influence of visible light reached 81.35%, which was superior to  $\text{g-C}_3\text{N}_4/\text{PVDF}$  (46.07%) and  $\text{SiO}_2/\text{PVDF}$  (14.79%). Therefore, this study is expected to expand the prospects in the field of membrane filtration technology.

**Keywords:**  $\text{SiO}_2$ ,  $\text{g-C}_3\text{N}_4$ ,  $\text{SiO}_2/\text{g-C}_3\text{N}_4$ , PVDF

## 1. INTRODUCTION

Water pollution by persistent organic compounds - dyes, pesticides, and pharmaceutical residues - is becoming one of today's most serious environmental challenges. These compounds are often highly toxic, difficult to biodegrade, and persistent in the environment, requiring effective and ecologically friendly treatment methods.<sup>1</sup> Among modern treatment technologies, heterogeneous photocatalysis under visible light is a promising method because it completely decomposes organic pollutants into non-toxic products such as  $\text{CO}_2$  and  $\text{H}_2\text{O}$  without leaving secondary residues.<sup>2</sup> In the field of photocatalytic materials, graphitic carbon nitride ( $\text{g-C}_3\text{N}_4$ ) is considered a potential candidate due to its narrow band gap ( $\sim 2.7$  eV), good visible light absorption, high chemical stability, and simple synthesis from precursors such as melamine or urea.<sup>3</sup> However,  $\text{g-C}_3\text{N}_4$  has limitations, typically low surface area, poor adsorption capacity, and fast recombination rate of electron–hole pairs, which make the photocatalytic efficiency low: high chemical stability and simple synthesis from precursors such as melamine or urea.<sup>4</sup> To improve the catalytic efficiency, synthesizing composite materials between  $\text{g-C}_3\text{N}_4$  and supporting materials is considered an effective strategy. Silicon dioxide ( $\text{SiO}_2$ ) - with its porous

structure, large surface area, and high stability - not only enhances the dispersion of  $\text{g-C}_3\text{N}_4$  but also improves the charge transfer process in the photocatalytic reaction.<sup>5,6</sup> In addition, poly(vinylidene fluoride) (PVDF) is a chemically stable fluoropolymer, good mechanical properties and easy to process into films, very suitable as a substrate for membrane-based photocatalyst systems, helping to improve applicability and reusability.<sup>7</sup>

For the above reasons, the development of  $\text{SiO}_2/\text{g-C}_3\text{N}_4/\text{PVDF}$  composite materials has significant scientific and practical significance, aiming at enhancing photocatalytic activity under visible light, while improving the stability and recovery of materials after treatment. This study focuses on the synthesis, chemical characterization, and evaluation of the treatment performance of  $\text{SiO}_2/\text{g-C}_3\text{N}_4/\text{PVDF}$  materials for typical organic compounds in wastewater, elucidating the relationship between material structure and photocatalytic efficiency.

## 2. EXPERIMENTAL

### 2.1. Material synthesis

**Chemicals:** All chemicals used for material synthesis include urea ( $(\text{NH}_2)_2\text{CO}$ ), TEOS (Tetraethyl orthosilicate) ( $\text{C}_8\text{H}_{20}\text{O}_4\text{Si}$ ), CTAB (Hexadecyl trimethyl ammonium bromide), ( $[(\text{C}_{16}\text{H}_{33})\text{N}(\text{CH}_3)_3]\text{Br}$ ), polyvinylidene fluoride (PVDF), N-Methy-2-

pyrrolidone (NMP) and rhodamine B ( $C_{28}H_{31}ClN_2O_3$ ), Merck.

## 2.2. Materials synthesis:

### 2.2.1. Synthesis of $g\text{-}C_3N_4$ material

Put 10 grams of finely ground urea into a ceramic cup and cover it tightly with aluminum foil. Place in furnace, heat to 550 °C for 1 hour. The solid obtained was pale yellow, washed with distilled water and ethanol, then dried at 80 °C for 12 hours. The product is finely ground and marked  $g\text{-}C_3N_4$ .

### 2.2.2. Synthesis of $SiO_2$ material

Add 0.16 g of hexadecyl trimethyl ammonium bromide (CTAB) to 50 mL of distilled water, then slowly add 15 mL of ethanol and 1 mL of solution. Stir for 0.5 hour, slowly add 1 mL tetraethyl orthosilicate (TEOS) dropwise into the solution, and stir for 24 hours. The obtained product was washed with deionized water and ethanol three times, dried for 24 h at 60 °C, and denoted  $SiO_2$ .

### 2.2.3. Synthesis of $SiO_2/g\text{-}C_3N_4$ composite material

Put 0.1g  $SiO_2$  and 3g urea into an agate mortar and grind finely. Then put the solid mixture into a ceramic cup, cover it tightly, and heat it in an inert Ar gas environment at 550 °C for 1 hour. Cool to room temperature, grind and wash the sample with distilled water until neutral. The solid was dried at 80 °C for 12 hours and denoted as  $SiO_2/g\text{-}C_3N_4$ .

### 2.2.4. Synthesis of $SiO_2/g\text{-}C_3N_4/PVDF$ material

Put 0.1g of  $SiO_2/g\text{-}C_3N_4$  material into a glass jar with a lid, add 5 mL of NMP solution, and sonicate for 10 minutes. Then stir well on a magnetic stirrer for 30 minutes. Continue ultrasonic vibration for another 20 minutes and stir evenly on a magnetic stirrer for 20 minutes. Continue ultrasonic vibration for another 20 minutes and stir evenly on a magnetic stirrer for 20 minutes. Then let the mixture sit for 3 hours. Using a stainless steel scraper (250  $\mu m$  x 15 cm), roll the mixture evenly onto the glass to form a composite film, quickly put the glass with the film into water to perform the phase reversal process, and the material is denoted as  $SiO_2/g\text{-}C_3N_4/PVDF$ .

## 2.3. Material characterization

The synthesized materials were characterized using several techniques. Infrared spectroscopy IR was performed on a Shimadzu IR Prestige-21. The crystal phase was analyzed

by X-ray diffraction (XRD) using a Siemens D-500 Bruker system. Scanning electron microscopy (SEM) and X-ray energy dispersive spectroscopy (EDS) were conducted using a JSM-7600F device. Photoluminescence (PL) spectra were measured on a Hitachi F-7000 instrument with an excitation wavelength of 360 nm.

## 2.4. Photocatalytic evaluation

The photocatalytic activity of the obtained materials was evaluated by the decomposition of Rhodamine B (RhB) in an aqueous solution under visible light irradiation. Materials containing 0.1 g of the photocatalyst were added to 100 mL of RhB solution with a concentration of 10 mg/L and stirred in the dark for 60 minutes to achieve adsorption-desorption equilibrium. The photocatalytic process was then initiated under a 40W LED light. Every 30 minutes, 7 mL of the solution was centrifuged to remove the solid part. The concentration of RhB in the solution was determined on a UV-Vis meter (CE-2011) at a wavelength of 553 nm.

## 3. RESULTS AND DISCUSSION

### 3.1. Material characteristics

The crystal structures and phase compositions of the synthesized  $SiO_2$ ,  $g\text{-}C_3N_4$ ,  $SiO_2/g\text{-}C_3N_4$  powders, and PVDF,  $SiO_2/PVDF$ ,  $g\text{-}C_3N_4/PVDF$ , and  $SiO_2/g\text{-}C_3N_4/PVDF$  films are shown in Figure 1.

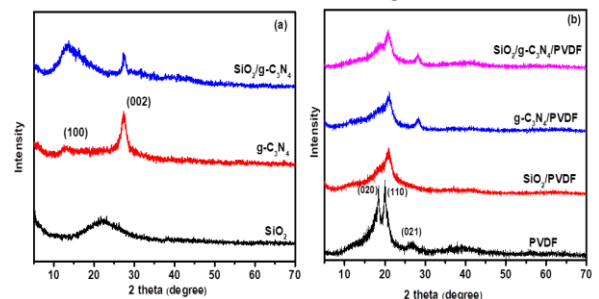


**Figure 1.** (a) XRD patterns of  $SiO_2$ ,  $g\text{-}C_3N_4$  and (b) PVDF,  $SiO_2/PVDF$ ,  $g\text{-}C_3N_4/PVDF$  and  $SiO_2/g\text{-}C_3N_4/PVDF$ .

Figure 1a shows that the  $SiO_2$  material exhibits a broad peak at  $2\theta \approx 23^\circ$  corresponding to the amorphous nature of  $SiO_2$ .<sup>8</sup>  $g\text{-}C_3N_4$  shows typical diffraction peaks corresponding to the (002) and (100) planes of  $g\text{-}C_3N_4$ .<sup>9</sup> Specifically, the peak at  $2\theta = 13.5^\circ$  can be attributed to the in-plane structural stacking motif in the tri-s-triazine (s-heptazine)-based structure of  $g\text{-}C_3N_4$ , while the strong diffraction peak located at  $2\theta = 27.6^\circ$  is a result of the inter-plane stacking of the conjugated aromatic units of  $g\text{-}C_3N_4$ .<sup>10</sup> XRD results of  $SiO_2/g\text{-}C_3N_4$  composite material fully show the

characteristic peaks of both  $\text{g-C}_3\text{N}_4$  and  $\text{SiO}_2$ . The  $\text{SiO}_2$  peak at  $23^\circ$  is not clearly shown in the composite sample, possibly due to the amorphous  $\text{SiO}_2$  structure and the stacking of  $\text{g-C}_3\text{N}_4$ . Thus, the  $\text{SiO}_2$  added to the  $\text{g-C}_3\text{N}_4$  substrate does not change the crystal structure. The results in Figure 1b show that PVDF has 3 characteristic peaks at  $18.5^\circ$ ,  $20.1^\circ$ ,  $26.7^\circ$  corresponding to the planes (020), (110), (021). When dispersing  $\text{g-C}_3\text{N}_4$ ,  $\text{SiO}_2$ ,  $\text{SiO}_2/\text{g-C}_3\text{N}_4$  onto PVDF polymer matrix, the PVDF peaks still appear at almost the same position but the intensity is reduced. For the  $\text{g-C}_3\text{N}_4/\text{PVDF}$  sample, a characteristic strong peak at  $27.6^\circ$  and a weak peak at  $13.5^\circ$  corresponding to the (002) and (100) reflection planes of graphite-structured materials appear.<sup>11</sup>

Figure 2 shows the FT-IR spectrum of the synthesized material samples, demonstrating no change in the PVDF polymer structure.

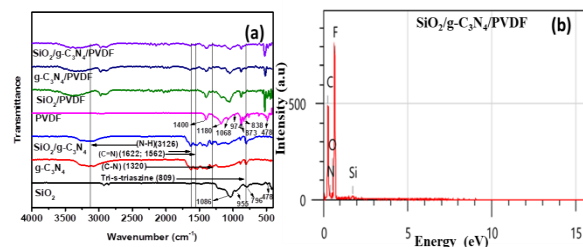


**Figure 2.** (a) FT-IR spectra of  $\text{SiO}_2$ ,  $\text{g-C}_3\text{N}_4$ ,  $\text{SiO}_2/\text{g-C}_3\text{N}_4$ , PVDF,  $\text{SiO}_2/\text{PVDF}$ ,  $\text{g-C}_3\text{N}_4/\text{PVDF}$ ,  $\text{SiO}_2/\text{g-C}_3\text{N}_4/\text{PVDF}$ , and (b) EDX spectra of  $\text{SiO}_2/\text{g-C}_3\text{N}_4/\text{PVDF}$ .

The FT-IR spectrum of pure PVDF shows the combination of  $\alpha$  and  $\beta$  phases. The characteristic absorption bands for the  $\alpha$  form are 1180 and 974  $\text{cm}^{-1}$ , and for the  $\beta$  form are 1400, 1068, 873, and 838  $\text{cm}^{-1}$ . The absorption bands at 1400, 873  $\text{cm}^{-1}$  represent the valence vibration of the C-F bond, at 1180 and 487  $\text{cm}^{-1}$  represent the C-C bond and the bending vibration of  $\text{CF}_2$ . These absorption bands are present in all FT-IR spectra of the material films without any structural changes, which may be caused by chemical bonding. Furthermore, the FT-IR spectra of  $\text{SiO}_2/\text{PVDF}$  and  $\text{g-C}_3\text{N}_4/\text{PVDF}$  materials showed characteristic absorption bands for  $\text{g-C}_3\text{N}_4$  and  $\text{SiO}_2$ . Typical absorption bands for  $\text{g-C}_3\text{N}_4$  are located at 3126  $\text{cm}^{-1}$  corresponding to N-H groups, at 1622 and 1562  $\text{cm}^{-1}$  belonging to C=N bonds, at 1320  $\text{cm}^{-1}$  corresponding to C-H bonds, and the absorption band at 809  $\text{cm}^{-1}$  corresponding to tri-s-triazine units.<sup>12</sup>

In the IR spectrum of  $\text{SiO}_2$ , strong absorption bands appear at wave numbers 1086,

955, and 796  $\text{cm}^{-1}$  corresponding to the bonds of Si-O-Si, the deformation vibration of Si-OH, and the symmetric valence vibration of the Si-O bond. The peak observed at 478  $\text{cm}^{-1}$  in the composite film material is related to the Si-O-Si stretching vibration of  $\text{SiO}_2$ .<sup>13</sup>

SEM images show a clear difference in the distribution of materials on the polymer membrane. PVDF material (Figure 3a) has a reasonably smooth surface with a uniform surface structure and is applied as a good substrate membrane. Figure 3b shows that the  $\text{SiO}_2$  particles are relatively uniformly distributed in the PVDF matrix. The surface of the material becomes more porous and increases the surface area. The  $\text{g-C}_3\text{N}_4$  material is in sheet form, so when dispersed on the PVDF substrate (Figure 3c), it creates density heterogeneity, large particle clusters, uneven structure, and increases the material's porosity. The combination of  $\text{SiO}_2$  and  $\text{g-C}_3\text{N}_4$  (Figure 3d) shows a significantly more porous surface, showing dispersed phases and many defect sites. This improves the photocatalytic properties, mechanical strength, and membrane permeability.

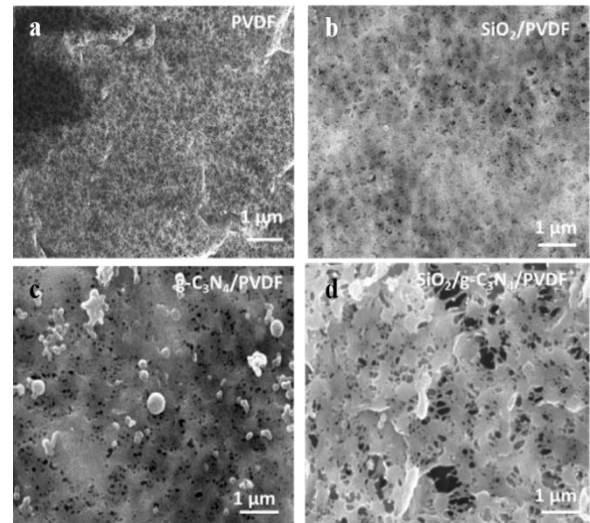


**Figure 3.** SEM images of PVDF (a),  $\text{SiO}_2/\text{PVDF}$  (b),  $\text{g-C}_3\text{N}_4/\text{PVDF}$  (c),  $\text{SiO}_2/\text{g-C}_3\text{N}_4/\text{PVDF}$  (d).

Energy dispersive X-ray (EDX) spectrum was characterized for the  $\text{SiO}_2/\text{g-C}_3\text{N}_4/\text{PVDF}$  composite sample (Figure 2b). The results from EDX images show the full presence of elements F, C, O, Si, and N in the sample, proving the successful synthesis of the material.

PL spectra of the materials were performed with an excitation wavelength of 390 nm at room temperature to study the

photogenerated electron-hole recombination, and solid UV-Vis spectra determined the band gap energy of the materials, as shown in Figure 4.

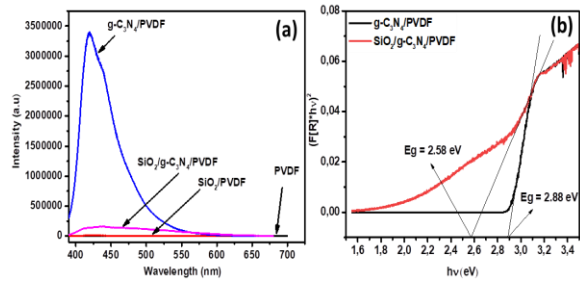


**Figure 4.** (a) PL spectra of  $\text{g-C}_3\text{N}_4/\text{PVDF}$ ,  $\text{SiO}_2/\text{PVDF}$ , PVDF,  $\text{SiO}_2/\text{g-C}_3\text{N}_4/\text{PVDF}$  (a) and (b) Band gap energy of  $\text{g-C}_3\text{N}_4/\text{PVDF}$ ,  $\text{SiO}_2/\text{g-C}_3\text{N}_4/\text{PVDF}$ .

For PVDF, no PL intensity was observed over the entire spectral range. The  $\text{g-C}_3\text{N}_4$  particles dispersed on the PVDF membrane have a maximum intensity corresponding to a wavelength of 419 nm, where the molecules with amino groups, such as  $\text{g-C}_3\text{N}_4$ , the nucleophile attack of the amino group on the carbon atom will lead to the nucleophile substitution of fluorine to form a covalent bond between PVDF and  $\text{g-C}_3\text{N}_4$ . The observed PL intensity of  $\text{g-C}_3\text{N}_4$  is higher, which indicates a faster recombination rate between photogenerated electrons and holes. As for the PL spectrum of  $\text{SiO}_2/\text{PVDF}$ , the emission intensity is very low, almost equivalent to the PL spectrum of PVDF. This is explained by the fact that  $\text{SiO}_2$  has a significant band gap energy and poor photocatalytic activity in the visible light region. On the other hand, the PL spectrum of the  $\text{SiO}_2/\text{g-C}_3\text{N}_4/\text{PVDF}$  composite material has a reduced fluorescence emission intensity compared to  $\text{g-C}_3\text{N}_4/\text{PVDF}$  (Figure 4a) and the band gap energy of the  $\text{SiO}_2/\text{g-C}_3\text{N}_4/\text{PVDF}$  material ( $E_g = 2.58 \text{ eV}$ ) is lower than that of  $\text{g-C}_3\text{N}_4/\text{PVDF}$  ( $E_g = 2.88 \text{ eV}$ ) (Figure 4b). Therefore, when there is radiation, electrons move from  $\text{g-C}_3\text{N}_4$  to the conduction band of  $\text{SiO}_2$  and then quickly move to the catalyst's surface to perform a reduction reaction with oxygen molecules, limiting the ability to recombine.

### 3.2. Photocatalytic performance

The results of the photocatalytic evaluation for PVDF,  $\text{g-C}_3\text{N}_4/\text{PVDF}$ , and  $\text{C}/\text{g-C}_3\text{N}_4/\text{PVDF}$  are shown in Figure 5.

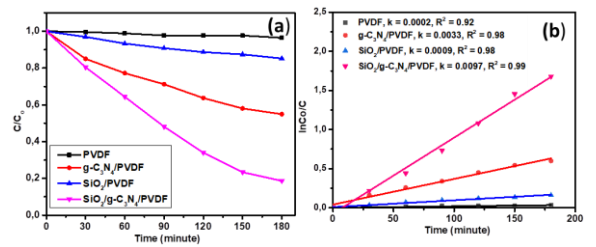


**Figure 5.** (a) RhB decomposition and (b) pseudo-first-order kinetic model under visible light of  $\text{g-C}_3\text{N}_4/\text{PVDF}$ ,  $\text{SiO}_2/\text{g-C}_3\text{N}_4/\text{PVDF}$ , and  $\text{SiO}_2/\text{g-C}_3\text{N}_4/\text{PVDF}$ .

The graph shows that after 180 minutes of illumination under a 40W LED lamp, the decomposition efficiency of RhB solution of  $\text{SiO}_2/\text{g-C}_3\text{N}_4/\text{PVDF}$  sample is the highest at 81.35%, the materials  $\text{g-C}_3\text{N}_4/\text{PVDF}$ ,  $\text{SiO}_2/\text{PVDF}$  have decomposition efficiency of 46.07% and 14.79% respectively. This may be because the band gap energy of the  $\text{SiO}_2/\text{g-C}_3\text{N}_4/\text{PVDF}$  material (2.58 eV) is lower than the band gap energy of the  $\text{g-C}_3\text{N}_4$  material (2.88 eV), which makes the ability to separate and move photogenerated electrons and holes to the material surface to perform reactions faster, limiting the ability to recombine between charge carriers.  $\text{SiO}_2/\text{PVDF}$  material works well in the ultraviolet region, which is understandable because the photocatalytic efficiency in the visible light region is only 14.79%. The PVDF membrane alone did not show photocatalytic activity, indicating that the photocatalytic activity was due to the composite material; the single dispersed materials were exhibited. The kinetic model of RhB degradation of  $\text{SiO}_2/\text{g-C}_3\text{N}_4/\text{PVDF}$  material has a rate constant of  $0.00797 \text{ (min}^{-1}\text{)}$  which is much larger than that of  $\text{g-C}_3\text{N}_4/\text{PVDF}$  and  $\text{SiO}_2/\text{PVDF}$  materials ( $0.0033$  and  $0.0009 \text{ min}^{-1}$ ) (Figure 5b). This result confirms the potential application of  $\text{SiO}_2/\text{g-C}_3\text{N}_4/\text{PVDF}$  material in the treatment of organic pollutants under visible light in aquatic environments.

## 4. CONCLUSION

In this study, PVDF composite films modified with  $\text{SiO}_2$  and  $\text{g-C}_3\text{N}_4$  were successfully synthesized. XRD and FT-IR results showed that the incorporation of fillers did not change PVDF's crystal structure and polymer framework. The surface morphology is significantly improved with the appearance of a porous structure and a uniformly dispersed phase. PL spectrum and band gap analysis showed that the  $\text{SiO}_2/\text{g-C}_3\text{N}_4/\text{PVDF}$  sample can inhibit  $\text{e}^-/\text{h}^+$  recombination, and the band gap is

suitable for visible light absorption. Photocatalytic testing showed that the  $\text{SiO}_2/\text{g-C}_3\text{N}_4/\text{PVDF}$  sample had the highest RhB degradation efficiency (81.35%), confirming its potential application in organic pollution treatment under visible light.

### Acknowledgments

### REFERENCES

1. Zhang, L., Zhao, X., & Chen, G. Recent advances in visible-light-driven photocatalytic degradation of organic pollutants, *Applied Catalysis B: Environmental*, **2020**, *261*, 118201.

2. Hongxia Lin, J. W., Fan Zhou, Xiaolong Zhao, Pengfei Lu, Guanghui Sun, Yuhua Song, Yayun Li, Xiaoyong Liu, Hongxing Dai. Graphitic carbon nitride-based photocatalysts in the applications of environmental catalysis, *Journal of Environmental Sciences*, **2023**, *124*, 570-590.

3. T.K.A. Nguyen, T. T. P., N.P. Huy, E.W. Shin. The effect of graphitic carbon nitride precursors on the photocatalytic dye degradation of water-dispersible graphitic carbon nitride photocatalysts, *Appl. Surf. Sci.*, **2021**, *537*, 148027-148038.

4. Yutang Yu, H. H. Coupled adsorption and photocatalysis of  $\text{g-C}_3\text{N}_4$  based composites: Material synthesis, mechanism, and environmental applications, *Chemical Engineering Journal*, **2023**, *453*, 139755.

5. Qiang Hao, X. N., Changshun Nie, Simeng Hao, Wei Zou, Jiangman Ge, Daimei Chen, and Wenqing Yao. Highly Efficient  $\text{g-C}_3\text{N}_4/\text{SiO}_2$  Heterojunction: The role of  $\text{SiO}_2$  for the Enhanced Visible Light Photocatalytic Activity, *Phys. Chem. Chem. Phys.*, **2016**, *18* (1-25).

6. Xiaoxing Wang, S. W., Wenda Hu, Wenda Hu, Jun Cai, Lihong Zhang, Lvzhuo Dong, Zhao Leihong, Yiming He. Synthesis and photocatalytic activity of  $\text{SiO}_2/\text{g-C}_3\text{N}_4$  composite photocatalyst, *Materials Letters*, **2014**, *115*, 53-56.

7. Iryna Kolesnyk, J. K., Halyna Bubela, Viktoriia Konovalova, Anatolii Burban, ; Aleksandra Cyganiuk, W. K. Photocatalytic properties of PVDF membranes modified with  $\text{g-C}_3\text{N}_4$  in the process of Rhodamines decomposition, *Separation and Purification Technology*, **2020**, *250*, 117231.

8. Prakash, K.; Kumar, P. S.; Latha, P.; Saravanakumar, K.; Karuthapandian, S. Design and fabrication of a novel metal-free  $\text{SiO}_2/\text{gC}_3\text{N}_4$  nanocomposite: a robust photocatalyst for the degradation of organic contaminants, *Journal of Inorganic and Organometallic Polymers and Materials*, **2018**, *28*, 268-278.

9. Shen, Y.; Guo, X.; Bo, X.; Wang, Y.; Guo, X.; Xie, M.; Guo, X. Effect of template-induced surface species on electronic structure and photocatalytic activity of  $\text{g-C}_3\text{N}_4$ , *Applied Surface Science*, **2017**, *396*, 933-938.

10. Mo, Z.; She, X.; Li, Y.; Liu, L.; Huang, L.; Chen, Z.; Zhang, Q.; Xu, H.; Li, H. Synthesis of  $\text{g-C}_3\text{N}_4$  at different temperatures for superior visible/UV photocatalytic performance and photoelectrochemical sensing of MB solution, *RSC advances*, **2015**, *5* (123), 101552-101562.

11. Zhu, B.; Xia, P.; Li, Y.; Ho, W.; Yu, J. Fabrication and photocatalytic activity enhanced mechanism of direct Z-scheme  $\text{g-C}_3\text{N}_4/\text{Ag}_2\text{WO}_4$  photocatalyst, *Applied Surface Science*, **2017**, *391*, 175-183.

12. Vilamova, Z.; Czernek, P.; Zagora, J.; Svoboda, L.; Bednar, J.; Simonova, Z.; Placha, D.; Dvorsky, R. Fibrous PVDF membranes modified by anchored  $\text{g-C}_3\text{N}_4@\text{GO}$  composite with enhanced photocatalytic activity, *Applied Surface Science*, **2024**, *677*, 161055.

13. Kim, Y.-J.; Ahn, C. H.; Lee, M. B.; Choi, M.-S. Characteristics of electrospun PVDF/ $\text{SiO}_2$  composite nanofiber membranes as polymer electrolyte, *Materials Chemistry and Physics*, **2011**, *127* (1-2), 137-142.